Phase field simulations of polarization switching-induced toughening in ferroelectric ceramics

Jie Wang and Tong-Yi Zhang*

Department of Mechanical Engineering
Hong Kong University of Science and Technology
Clear Water Bay, Kowloon, Hong Kong, China

Polarization switching-induced shielding or anti-shielding of an electrically permeable crack in a mono-domain ferroelectric material with the original polarization direction perpendicular to the crack is simulated by a phase field model based on the time-dependent Ginzburg-Landau equation. The domain wall energy and the long-range mechanical and electrical interactions between polarizations are taken into account. The phase field simulations exhibit a wing-shape- switched zone backwards the crack tip. The polarization switching-induced internal stresses shield the crack tip from applied mechanical loads. A local J-integral is numerically calculated and used as a failure criterion to illustrate the polarization switching-toughening. The result indicates that an applied uniform electric field parallel to the original polarization direction reduces the apparent fracture toughness, while an applied uniform electric field anti-parallel to the original polarization direction enhances it.

Keywords: Phase field modeling, Polarization switching, Fracture, Ferroelectricity, Microstructure

* Corresponding author, Tel: (852) 2358-7192, Fax: (852) 2358-1543, E-mail: mezhangt@ust.hk

1. Introduction

Ferroelectric ceramics have attracted much attention due to their pronounced dielectric, piezoelectric, and pyroelectric properties. However, ferroelectric ceramics are brittle and susceptible to cracking at all scales ranging from electric domains to devices. The fracture behavior of ferroelectric ceramics is complex under mechanical and/or electric loading. The theoretical results based linear piezoelectric fracture mechanics cannot predict the experimental observations of the fracture behavior of ferroelectric ceramics under combined mechanical and electrical loading [1-4]. It is still debated in the fracture mechanics community whether an applied electric field impedes or enhances the propagation of an electrically insulting crack in a ferroelectric ceramic material. The complex failure behavior of ferroelectric ceramics is attributed to the coherent nonlinear coupling between the mechanical and electric fields. Under mechanical and/or electrical loading, the intensified stress and electric fields in the vicinity of a crack may cause polarization switching, thereby changing the local electrical domain structure. The change in the local domain structure, in turn, changes the internal electric field near the crack tip and the internal stress field because spontaneous strains are accompanied with polarizations. The switching-induced internal stress field may, depending on the nature of the internal stress, shield or anti-shield the crack tip from the applied mechanical load, resulting in switching-toughening or switching-weakening [5]. Switching-toughening may be regarded as a kind of phase-transformation-toughening. Following the classical phase-transformation-toughening theory [6], theoretical studies [7-14] have been conducted to understand and predict the polarization switching-induced toughening under mechanical and/or electrical loading. In the previous studies, the switching was considered at the length scale of electric domains. An electric domain, modeled as an inclusion, can switch 90° or 180°, which is normally called the 90°- or 180°-domain switching. Whether a 90°- or 180°-domain switching of an individual domain will

occur is based on a preset switching criterion. The switching criterion is established by calculating the change in a thermodynamic energy before and after the switching. If the change exceeds a critical value, domain switching occurs. Otherwise, domain switching will not occur. For example, the switching criteria proposed by Hwang et al. [8] state that a 180°-switching, where stresses are irrelevant, is activated if

$$E_i \Delta P_i \geq 2 P_s E_c , \tag{1}$$

where E_i and P_i are the electric field strength and the polarization vectors, respectively, P_s is the saturated magnitude of polarization, E_c is the absolute value of the coercive field, and the Δ denotes a change of a property before and after the switching. The 90°-switching criterion includes the work done by mechanical stresses,

$$\sigma_{ij} \Delta \varepsilon_{ij} + E_i \Delta P_i \geq 2 P_s E_c , \tag{2}$$

where σ_{ij} and ε_{ij} denote the stress and the strain tensors, respectively. Note that 90°-switching may occur without the presence of external electric fields. Eqs. (1) and (2) represent typically simplified versions of thermodynamic energy-based switching criteria, where the saturated magnitude of polarization is assumed to be constant. In the study of domain switching-induced toughening, a switched zone in front of a crack tip under given mechanical and/or electric loads is determined based on the switching criterion. Then, a local mode I stress intensity or a local energy release rate is calculated at the crack tip. Finally, the local stress intensity or the local energy release rate is used as the failure criterion to study the shielding or anti-shielding effect and the toughening behavior. Obviously, domain switching criteria depend on the used thermodynamic energy, which closely linked to the constitutive law. For instance, the domain-switching-induced enhancement of the steady state fracture toughness in a polycrystalline ferroelastic ceramic was analyzed with a phenomenological constitutive law [9] to account for the strain saturation, asymmetry in tension versus

compression, Bauschinger effects, reverse switching and strain reorientation. In the analysis [9], the crack growth was assumed to proceed at a critical level of the local mechanical energy release rate.

In the theoretical research on fracture of ferroelectric ceramics, there is a crucial issue about the electric boundary condition along the surfaces of an electric insulating crack. Two approximate electric boundary conditions are commonly adopted in the theoretical research, namely the electrically permeable and impermeable boundary conditions. The experimental measurements of electric field distributions in a pre-cracked ferroelectric ceramic sample [15] indicate that the electrically permeable boundary condition may be more appropriate. In the present study, therefore, we shall investigate an electrically permeable crack.

Phase field simulations are based on fundamental principles of thermodynamics and kinetics, which provide a powerful method for predicting the temporal evolution of microstructures in materials. In a phase field model, thermodynamic energies are described in terms of a set of continuous order parameters. The temporal evolution of a microstructure is obtained by solving kinetics equations that govern the time-dependence of the spatially inhomogeneous order parameters. A phase field model does not make any prior assumptions about transient microstructures, which may appear during a phase transformation path, and about transformation criteria. Phase transformation is a direct consequence of the minimization process of the total free energy of an entire simulated system. Phase field simulations have been conducted to study domain structures in ferroelectric materials and polarization switching under electric and/or mechanical loading [16-23]. The object of the present study is to investigate the polarization switching-induced toughening of an electrically permeable crack by phase field simulations. Compared with the domain switching

models mentioned above [7-14], phase field simulations do not need any pre-established switching criteria. Polarization switching is a natural process occurring during the minimization of the total free energy of the entire simulated ferroelectric with given boundary and loading conditions. The polarization gradient energy is usually taken into account in phase field simulations of ferroelectric ceramics to represent the domain wall energy so that an electric domain structure is formed or changed automatically during the simulations. The previous phase field simulations of polarization switching [17] indicate that the macroscopic reversal of polarization does not simply imply a microscopic 180°-switching of electric domains, while remaining the original domain structure unchanged. Rather, the minimization of the free energy of the entire simulated system under external electric and/or mechanical loads changes the domain structure completely [17]. The temporal evolution of polarization switching shows that the domain switching is a kinetic process of the disappearance of the old domain structure and the nucleation and growth of a new domain structure, in which the new domain growth is accomplished mainly through domain wall motion. Not only are the directions of the domains after switching different from those of the original domains, but the domain size and configuration are also different. The domain structure is completely changed after the switch.

To simplify numerical calculations, periodic boundary conditions are usually employed in phase field simulations of ferroelectrics with the highly efficient Fast Fourier Transform technique such that elastic solution for a given polarization distribution can be obtained analytically in reciprocal space. However, periodic boundary conditions may be inappropriate in simulations of polarization switching-induced toughening because the boundary conditions are, in general, not periodic when only a crack is considered. In phase field simulations of nanoferroelectric ceramics, we have considered the long-range electrostatic and elastic

interactions without using periodic boundary conditions [24]. The numerical methods used in the previous work [24] are used here. For readers' convenience, a brief description of the used equations for the phase field simulations is given in Appendix A.

2. Phase field model

Two-dimensional simulations with plane strain condition along the third direction are conducted in the present study. We consider an electrically permeable crack lying inside an infinite ferroelectric single crystal under remote electric and/or mechanical loading, as shown in Fig.1 (a). Only a small rectangle area near the crack tip is taken as the simulated system, as shown in Fig.1 (b). Before applying any electric and mechanical loads, the simulated system is assumed to be a single electric domain with its polarization direction perpendicular to the crack direction. In the simulated system, spontaneous polarizations associated with spontaneous strains are embedded in a background material, i.e., in the paraelectric phase material. The spontaneous polarization vector, $\mathbf{P}=(P_1, P_2, P_3)$, is used as the order parameter to calculate the total free energy of the simulated ferroelectric system. The total free energy includes the standard Landau - Devonshire energy, the polarization gradient energy, the depolarization energy, and the electrical energy density due to an applied electric field. These energies are described in details in the Appendix. Under given applied electric and/or mechanical loads, the temporal evolution of the spontaneous polarization field is described by the time-dependent Ginzburg-Landau equation,

$$\frac{\partial P_i(\mathbf{r},t)}{\partial t} = -L\frac{\delta F}{\delta P_i(\mathbf{r},t)} \qquad (i=1, 2, 3), \tag{3}$$

where L is the kinetic coefficient, F is the total free energy, $\delta F / \delta P_i(\mathbf{r},t)$ represents the thermodynamic driving force of the spatial and temporal evolution of the simulated system, t denotes time and $\mathbf{r} = (x_1, x_2, x_3)$ is the spatial vector. In two-dimensional simulations,

$\mathbf{P} = (P_1, P_2)$ and $\mathbf{r} = (x_1, x_2)$. In each of iterations of Eq. (3), the depolarization field and the internal stress field are calculated from the spontaneous polarization field determined in this iteration. This approach is called here the thermal-stress-like approach. During the course of iterations, the spontaneous polarization field, the depolarization field and the internal stress field are changed until a steady state is reached, while the applied electric and/or mechanical loads remain unchanged. With the thermal-stress-like approach, there is apparently no coupling between applied electric and/or mechanical loads. In this case, a uniform applied electric field remains uniform in the simulated system due to the electrically permeable approximation of the crack. On the other hand, the crack concentrates an applied mechanical field greatly in the crack tip. Thus, applied mechanical loads are given by a crack tip stress field in terms of a mode I stress intensity factor, K_{app}, i.e., $\sigma_{ij}^{a} = \frac{K_{app}}{\sqrt{2\pi r}} f_{ij}(\theta)$, where $f_{ij}(\theta)$ is also related to elastic constants for an anisotropic material (See Appendix for detail), r and θ denote the distance from the crack tip and the polar angle, respectively, as shown in Fig. 1(b).

The phase field simulations are conducted with fixed dimensions of the four edges of the simulated rectangular region because it represents a middle part of a large ferroelectric single crystal. This means that the size of the simulated region is fixed after accommodating the displacements induced by applied mechanical loads. For the same reason, the electric boundary condition along the four edges is $d\phi / dn = 0$ in solving the depolarization field, where n refers to a unit length in the outward normal direction of an edge of the rectangle region and ϕ is the electric potential of the depolarization field. Based on the same argument, the boundary condition, $d\mathbf{P} / dn = 0$, is used along the four edges of the simulated region in

solving the spontaneous polarization field of Eq. (3). The boundary conditions along the crack surfaces are electrically permeable and mechanically traction-free.

In the simulations including the finite element analysis, we use 241×180 discrete grids for the simulated region with a dimensionless cell size of $\Delta x_1^* = \Delta x_2^* = 1$, where one dimensionless length number represents one nanometer. The crack size is set to be one-element in width and 120 elements in length. Since the crack is electrically permeable, there are no differences in electric displacement across the crack surfaces. In this sense, the crack may be regarded to be electrically perfect but mechanically defect. We set elastic constants of the elements in the crack area to be zero to model the mechanical defect in the finite element analysis. After external electric and/or mechanical loads are applied to the simulated system, a random fluctuation is added to the originally homogeneous spontaneous polarizations to initiate the evolution process. The dimensionless time step is 0.04 and the polarization distribution reaches a steady state after 1000 step iterations. In the following, most results without mentioning the iteration steps imply that the results are obtained after 1000 step iterations for the steady state. The domain structure is represented by the spontaneous polarization field, in which spontaneous polarizations vary spatially and each spontaneous polarization is characterized by an electric dipole. The length and direction of the electric dipole denote the magnitude and direction of local polarization, respectively.

3. Simulation results and discussion

We consider an original mono-domain ferroelectric with original polarization perpendicular to the crack by assigning $P_1^* = 0$ and $P_2^* = -1$ to the original dimensionless polarizations. When a purely mechanical load is applied to the simulated ferroelectric, a polarization-switched zone is formed if the applied dimensionless stress intensity factor is

exceeds a critical value. Figures 2(a), 2(b) and 2(c) show the polarization distribution without any applied electric field under purely applied stress intensity factors of $K^*_{app} = 440$, $K^*_{app} = 500$ and $K^*_{app} = 560$, respectively, where the solid line indicates the crack. Under $K^*_{app} = 440$, some spontaneous polarizations near the crack tip are changed, to some extent, in magnitude and orientation, as shown in the zoom-in Fig. 3, but no distinct switched zone is formed, as illustrated in Fig. 2(a). A switched zone is formed under a high applied mechanical load, as shown in Figs. 2(b) and Fig. 2(c) for $K^*_{app} = 500$ and $K^*_{app} = 560$, respectively. Obviously, the larger the applied mechanical load is, the larger the switched zone will be. The shape of switched zone with two wings backwards is almost symmetric with respect to the crack, but the switching direction is asymmetric, as illustrated in detail in Fig. 4. The polarizations in the wing above the crack switch 90^o clockwise, while the polarizations in the wing below the crack switch 90^o anticlockwise. Fig. 4 also shows that the polarizations form head-to-tail arrangements after switching, which may be attributed to the long range electrostatic interaction. To reduce the polarization gradient energy, the polarization orientations change gradually from the un-switched region to the switched region, thereby resulting in domain walls between the two regions, as shown in Fig. 4.

Figures 5(a) – 5(f) illustrate the temporal evolution of polarization switching at iteration steps of n=50, 100, 200, 300, 500 and 1000 under a purely mechanical load of $K^*_{app} = 560$. To clearly show the detailed polarization structure, the scale in each figure may be different, as indicated by the grid numbers on the horizontal and vertical axes. The polarization switching is nucleated at the crack tip, as indicated in Fig. 5(a) for n=50. After 50 step evolutions, polarizations at the vicinity of the crack tip switch their orientations. The four or five polarizations near the crack tip adjacent to the upper or lower crack surface switch the

maximum degree and the degree of switching becomes smaller if the polarizations are away from the crack tip. Figures 5(b) and 5(c) show the polarization structure after 100 and 200 step evolutions, respectively. Obviously, the switched zone grows up in both the wing length direction and the wing width direction. Furthermore, the switched degree of the polarization inside the wing is larger after 200 evolutions than that after 50 step evolutions. It is interesting to note that after 300 step evolutions, the switched zone moves 2 or 3 grids backward the crack direction. There is a residual switched region, 2 or 3 grids back of the crack tip, adjacent or close to the upper or lower crack surface, as shown in Fig. 5(d). This phenomenon becomes more distinct after 500 step evolutions. The switched zone moves backward the crack direction by 7 or 8 grids, as illustrated in Fig. 5(e). Finally, the switched zone grows to its steady state after 1000 step evolutions. The switched zone looks like a pair of wings with a nose, as shown by Fig. 5(f).

Under combined mechanical and electric loading, the switched zone is different from that under purely mechanical loading. In the simulations, electric and mechanical loads are applied simultaneously. Figures 6(a), 6(b) and 6(c) show the polarization patterns under uniform electric fields of $E_2^{a,*} = -0.5$, $E_2^{a,*} = 0$ and $E_2^{a,*} = 0.5$, respectively, where $K_{app}^{*} = 560$. The size of the switched zone increases if the applied electric field is $E_2^{a,*} = 0.5$, whereas applying $E_2^{a,*} = -0.5$ reduces the size of the switched zone. As mentioned above, polarization switching generates an internal stress field and the total stresses include the applied stresses and the induced stresses. Figures 7(a) and 7(b) show the distributions of the total stresses, σ_{22}^{*} and σ_{12}^{*}, in front of crack tip along the x_1 axis, respectively, where the applied stresses are plotted as references. The total stress field equals the applied stress field before polarization switching because there are no induced internal stresses in the original simulated system due to homogeneous distributed polarizations. Figure 7(a) shows that the

σ_{22}^* stresses become smaller after the switching. Combining Fig. 6 with Fig. 7 indicates that the larger the switched zone is, the smaller the stress of σ_{22}^* will be. The reduction of the total σ_{22}^* stress means that the switching-induced internal stress shields the crack tip from the applied mechanical load, which will result in polarization switching-toughening. The polarization switching induces a shear stress, σ_{12}^*, in front of the crack, as shown by Fig. 7(b). Comparing the magnitude of σ_{12}^* to the magnitude of σ_{22}^* illustrates that at a given distance from the crack tip, the tensile stress is at least one order higher in magnitude than that of the shear stress, thereby indicating that the crack tip is still predominantly under mode I loading after the polarization switching. Nevertheless, the generation of the shear stress changes the original mode I crack to a mixed mode I+II crack. In this case, it may be more appropriate to take the local J-integral as the fracture criterion.

Following the thermal-stress-like approach, only the mechanical J-integral is calculated from

$$J = \int_s (\sigma_{ij}\varepsilon_{ij}/2)dx_2 - T_i \frac{\partial u_i}{\partial x_1} ds\,, \tag{4}$$

where $T_i = \sigma_{ij} n_j$ denotes the traction vector, σ_{ij} and ε_{ij}, u_i and n_j are total stresses, total stains, total displacements and cosines of unit outward normal vector, respectively. Without the polarization-switched zone, the J-integral is path-independent. We have numerically checked the path-independent behavior along a global integral contour, Γ_g, and a local integral contour, Γ_l, which are shown in Fig. 8 (a). As expected, the J-integral along Γ_g is 231.18 and along Γ_l is 224.46 under the purely mechanical load of $K_{app}^* = 560$ before the polarization switching. Both the J-integrals along Γ_g and along Γ_l are almost the same as the analytic value of J=222.93. The difference between them is attributed to the numerical

calculation error. After the polarization switching, the J-integral is also path-independent as long as the integral contour does not pass through the switched zone. To calculate the local J-integral, we use narrow contours enclosing the crack tip and excluding the switched zone with only five elements in the contour width and many elements in the contour length, as shown in Fig. 8 (b). The contour n+1 is two-element longer than the contour n and the contour 1 has only two elements in length in front of the crack tip. The global J-integral is also calculated along contour Γ_g, which encloses the crack tip and the whole switched zone, after the polarization switching. Figure 9 shows the J-integrals calculated along the local integral contours before and after polarization switching under purely mechanical load of $K_{app}^{*} = 560$. Excluding the switched zone, the local J-integrals are almost the same for all integral contours except slight deviations calculated along the first two contours. The slight deviation is due to the great variation of the tip stress field near the crack tip, which causes a relatively large error in the numerical calculations. The mean local J-integral is 223.36 before the polarization switching, the same as the applied, while the mean local J-integral is reduced to 108.18 after the switching. Furthermore, the global J-integral calculated along contour Γ_g after the polarization switching is 198.73. The difference of the global J-integrals between before and after polarization switching is attributed to the small simulation area. Theoretically, if the unswitched zone is sufficiently large, the global J-integrals should be equal before and after polarization switching.

Figure 10 shows that the local J-integrals after switching increase monotonically with the applied *J*-integral under purely mechanical loading. This behavior indicates that a purely mechanical load can eventually fracture a ferroelectric sample with the use of local J-integral as the failure criterion even polarization switching occurs at the crack tip. Although polarization switching may be treated as a kind of plastic deformation, its behavior differs

from the nominal plastic deformation. Based on the classical Dugdale model [25], the local J-integral is zero, independent of the level of applied load, as long as a plastic zone is formed near the crack tip.

As mentioned above, an applied electric field plays an important role in the fracture behavior of ferroelectric ceramics. In the present study, an applied electric field does not change the applied J-integral because the crack is electrically permeable. However, an applied electric field changes the size of the polarization-switched zone and then varies the local J-integral. Figure 11 illustrates the local J-integral under a uniform applied electric field parallel or anti-parallel to the original polarization direction and a mechanical load of J^{*}_{before}=223.36, in which the local J-integral is normalized by the applied J-integral to emphasize the electric effect. Without any applied electric field, the polarization switching reduces about half of the local J-integral under the purely mechanical load. The normalized local J-integral is larger as a negative (parallel to the original polarization direction) applied electric field increases its strength, whereas the normalized local J-integral is smaller as a positive (anti-parallel) electric field increases.

Applying the Griffith theory to the crack tip gives a failure criterion based on the local J-integral, which means that the crack will propagate if the local J-integral exceeds a critical value. In the present study, we arbitrarily take the critical value of local J-integral to be $J^{*}_{l,c} = 108.18$ under the purely mechanical load of $J^{0*}_{before,M} = 223.36$ to illustrate the effect of electric field on the fracture behavior of ferroelectric ceramics. With this failure criterion, the apparent toughness in terms of the applied J-integral is $J^{0*}_{before,M} = 223.36$ under purely mechanical loading. The apparent toughness in terms of the critical applied J-integral under combined electric and mechanical loading is determined by the phase field simulations. A

uniform electric field is applied first and remained unchanged. Then, the applied mechanical load, i.e., the applied J-integral, is increased or decreased step by step. Under each applied J-integral, the local J-integral is calculated and compared with the critical value. If the calculated local J-integral is higher than the critical value, the applied J-integral will be reduced, otherwise, increased. In this way, the apparent toughness, i.e., the critical value of applied J-integral, is determined as a function of the applied electric field, which is normalized by the value under purely mechanical loading and plotted in Figure 12. The result indicates that an applied uniform electric field parallel (negative) to the original polarization direction reduces the apparent fracture toughness, while an applied uniform electric field anti-parallel (positive) to the original polarization direction enhances it. Note that in the literature, an applied electric field parallel or anti-parallel to the poling direction is usually defined to be a positive or negative electric field. The phase field simulations are consistent with the experimental observations [1] and theoretical results [11].

The polarization switching under different applied uniform electric fields perpendicular to the original polarization direction is also simulated under the fixed applied stress field of $K^*_{app} = 560$. Figures 13(a), 13(b) and 13(c) show the polarization patterns under uniform electric fields of $E_1^{a,*} = -0.25$, $E_1^{a,*} = 0$ and $E_1^{a,*} = 0.25$, respectively. Under purely mechanical loading, the switched zone shape is almost symmetric with respect to the crack, but the polarizations in the wings above and below the crack switch $\mp 90^o$ clockwise, respectively, as shown in Fig. 13(b). Thus, applying an electric field of $E_1^{a,*} = -0.25$ enhances the polarizations in the wing above the crack and retards the polarizations in the wing below the crack. As a result, the switched zone becomes asymmetric with the applied perpendicular electric field of $E_1^{a,*} = -0.25$. The wing above the crack grows up, while the wing below the crack disappears, as illustrated in Fig. 13(a). Similarly, applying an electric

field of $E_1^{a,*} = 0.25$ enlarges the wing below the crack and destroyed the wing above the crack, as shown in Fig. 13(c). The disappearance of the wing below or above the crack under a negative or positive electric field is to reduce the electrical energy. This is because the polarizations parallel to the external electric field have lower energy than the polarizations anti-parallel to it.

Fig.14 gives local J-integral variation under different uniform electric fields perpendicular to the poling direction. It shows little influence of both positive and negative electric fields on the local J-integral.

4. Concluding remarks

In summary, polarization switching near a crack tip in a mono-domain ferroelectric is simulated by using a phase field model, which takes into account the polarization gradient energy and the long-range mechanical and electrical interactions between polarizations. The major advantage of the phase field simulations lies in that the polarization switching is the result of minimizing the total free energy of the simulated system, which does not need any pre-described switching criteria. The polarizations in the switched wing above the crack switch 90^o clockwise, while the polarizations in the wing below the crack switch 90^o anticlockwise. There are electric domain walls between the switched and un-switched zones. All polarizations follow the head-to-tail arrangements due to the polarization gradient energy and the long range electric interaction energy. Since the internal stress field induced by polarizations is calculated by the thermal-stress-like method, the polarization-switched zone likes a plastic zone in the elastic-plastic fracture mechanics. In this case, J-integral is purely mechanical and path-independent as long as the integration contour does not pass through the switched zone. The polarization switching changes an original mode I crack to a mixed mode

I+II crack with a predominant mode I component. At the moment, it is difficult to attribute the mode II component to numerical errors. In this sense, a local J-integral is numerically calculated and used as a fracture criterion. Base on the fracture criterion, the simulations illustrate that an applied uniform electric field parallel to the original polarization direction reduces the apparent fracture toughness, while an applied uniform electric field anti-parallel to the original polarization direction enhances it. The results are consistent with some experimental observations.

Acknowledgements

This work was fully supported by an RGC grant from the Research Grants Council of the Hong Kong Special Administrative Region, China. The authors thank Prof. C.M. Landis at Rice University for stimulated and suggestive discussion.

Appendix

Following the previous work [24], spontaneous polarizations associated with spontaneous strains are considered to be embedded in a paraelectric background material. Under an external electric field, **E**, the total polarization, $\mathbf{P}^{(t)}$, is divided into two components, the spontaneous polarization, $\mathbf{P}$, and the induced polarization, $\mathbf{P}^{(i)}$. For simplicity, the induced polarization may be assumed to be linearly proportional to the electric field [26]. In this case, the electric displacement vector, **D**, can be given by

$$\mathbf{D} = \varepsilon_0 \mathbf{E} + \mathbf{P}^{(t)} = \varepsilon_0 \mathbf{E} + \mathbf{P}^{(i)} + \mathbf{P} = \varepsilon_0 \kappa \mathbf{E} + \mathbf{P}, \tag{A1}$$

where $\varepsilon_0 = 8.85 \times 10^{-12}\ \mathrm{Fm}^{-1}$ is the dielectric constant of vacuum and $\kappa = \kappa_{11} = \kappa_{22} = \kappa_{33}$ and $\kappa_{ij} = 0\ (i \neq j)$ denotes the relative dielectric constant tensor of the background paraelectric material.

The standard Landau - Devonshire energy density is [27]

$$\begin{aligned} f_{LD}(P_i, \sigma_{ij}) = {} & \alpha_1(P_1^2 + P_2^2 + P_3^2) + \alpha_{11}(P_1^4 + P_2^4 + P_3^4) + \alpha_{12}(P_1^2P_2^2 + P_2^2P_3^2 + P_1^2P_3^2) \\ & + \alpha_{111}(P_1^6 + P_2^6 + P_3^6) + \alpha_{112}[(P_1^4(P_2^2 + P_3^2) + P_2^4(P_1^2 + P_3^2) + P_3^4(P_1^2 + P_2^2)] \\ & + \alpha_{123}P_1^2P_2^2P_3^2 - \tfrac{1}{2}s_{11}(\sigma_{11}^2 + \sigma_{22}^2 + \sigma_{33}^2) - s_{12}(\sigma_{11}\sigma_{22} + \sigma_{22}\sigma_{33} + \sigma_{11}\sigma_{33}) \\ & - \tfrac{1}{2}s_{44}(\sigma_{12}^2 + \sigma_{23}^2 + \sigma_{13}^2) - Q_{11}(\sigma_{11}P_1^2 + \sigma_{22}P_2^2 + \sigma_{33}P_3^2) - Q_{12}[\sigma_{11}(P_2^2 + P_3^2) \\ & + \sigma_{22}(P_1^2 + P_3^2) + \sigma_{33}(P_1^2 + P_2^2)] - Q_{44}(\sigma_{12}P_1P_2 + \sigma_{13}P_1P_3 + \sigma_{23}P_2P_3), \end{aligned} \tag{A2}$$

where $\alpha_1 = (T - T_0)/2\varepsilon_0 C_0$ is the dielectric stiffness, $\alpha_{11}, \alpha_{12}, \alpha_{111}, \alpha_{112}, \alpha_{123}$ are higher order dielectric stiffnesses, T and T_0 denote temperature and the Curie-Weiss temperature, respectively, C_0 is the Curie constant; s_{ij} are the elastic compliance coefficients, Q_{ij} are electrostrictive constants and σ_{ij} denote mechanical stresses. Note that mechanical stresses include applied and internal stresses induced by spontaneous strains.

For ferroelectric materials, the polarization gradient energy represents also the domain wall energy. For simplicity, the lowest order of the gradient energy density is used here, which takes the form:

$$\begin{aligned} f_G(P_{i,j}) = & \frac{1}{2}G_{11}(P_{1,1}^2 + P_{2,2}^2 + P_{3,3}^2) + G_{12}(P_{1,1}P_{2,2} + P_{2,2}P_{3,3} + P_{1,1}P_{3,3}) \\ & + \frac{1}{2}G_{44}[(P_{1,2} + P_{2,1})^2 + (P_{2,3} + P_{3,2})^2 + (P_{1,3} + P_{3,1})^2] \\ & + \frac{1}{2}G'_{44}[(P_{1,2} - P_{2,1})^2 + (P_{2,3} - P_{3,2})^2 + (P_{1,3} - P_{3,1})^2], \end{aligned} \tag{A3}$$

where G_{11}, G_{12}, G_{44}, and G'_{44} are gradient energy coefficients, and $P_{i,j}$ denotes the derivative of the ith component of the polarization vector, P_i, with respect to the jth coordinate and i, j =1, 2, 3.

The total free energy includes the depolarization energy induced by spatially inhomogeneous spontaneous polarizations. The depolarization energy is a self-electrostatic energy corresponding to the long-range electrostatic interaction of spontaneous polarizations and is calculated by [28,29]

$$f_{dep} = -\tfrac{1}{2}(E_1^d P_1 + E_2^d P_2 + E_3^d P_3), \tag{A4}$$

where E_1^d, E_2^d and E_3^d are the components of depolarization field along the x_1, x_2 and x_3 axes, respectively. The self-electrostatic field is the negative gradient of the electrostatic potential, ϕ, induced by spontaneous polarizations, i.e., $E_i^d = -\phi_{,i}$. The electrostatic potential can be obtained by solving the following electrostatic equilibrium equation,

$$\mathbf{D}_{i,i} = (\varepsilon_0 \kappa \mathbf{E} + \mathbf{P})_{i,i} = 0 \text{ or } \varepsilon_0 \kappa(\phi_{,11} + \phi_{,22} + \phi_{,33}) = P_{1,1} + P_{2,2} + P_{3,3} \tag{A5}$$

for a body-charge-free paraelectric medium [30]. The polarization in Eq. (A5) is spontaneous polarization. If the total polarization is taken as order parameter, then the κ in Eq. (A5)

should be deleted. Equation (A5) is solved by using the finite difference method for a given polarization distribution.

If an externally electric field, E_i^a, is applied to the system, the applied field generates an additional electrical energy density,

$$f_{elec} = -E_i^a P_i . \tag{A6}$$

Integrating all free energy densities over the entire volume of a simulated ferroelectric material yields the total free energy, F, of the simulated ferroelectric material:

$$F = \int_V [f_{LD}(P_i, \sigma_{ij}) + f_G(P_{i,j}) + f_{dep}(P_i, E_i^d) + f_{elec}(P_i, E_i^a)] dV , \tag{A7}$$

where V denotes the volume of the simulated ferroelectric material.

In the present two-dimensional simulations, a uniform electric field, E_i^a, and/or a K_I tip stress field are applied to the simulated system. The tip stresses under a given K_{app} are expressed by [31]:

$$\sigma_{11}^a = \frac{K_{app}}{\sqrt{2\pi r}} \mathrm{Re}\left[\frac{s_1 s_2}{s_1 - s_2} \left(\frac{s_2}{(\cos\theta + s_2 \sin\theta)^{1/2}} - \frac{s_1}{(\cos\theta + s_1 \sin\theta)^{1/2}} \right) \right],$$

$$\sigma_{22}^a = \frac{K_{app}}{\sqrt{2\pi r}} \mathrm{Re}\left[\frac{1}{s_1 - s_2} \left(\frac{s_1}{(\cos\theta + s_2 \sin\theta)^{1/2}} - \frac{s_2}{(\cos\theta + s_1 \sin\theta)^{1/2}} \right) \right], \tag{A8}$$

$$\sigma_{12}^a = \frac{K_{app}}{\sqrt{2\pi r}} \mathrm{Re}\left[\frac{s_1 s_2}{s_1 - s_2} \left(\frac{1}{(\cos\theta + s_1 \sin\theta)^{1/2}} - \frac{1}{(\cos\theta + s_2 \sin\theta)^{1/2}} \right) \right].$$

In Eq. (A8) s_1 and s_2 are two unequal complex roots with positive imaginary parts of the characteristic equation

$$b_{11} s_i^{\,4} + (b_{12} + b_{44}) s_i^2 + b_{11} = 0 , \tag{A9}$$

in which

$$b_{11} = s_{11} - \frac{s_{12}^2}{s_{11}}, \quad b_{12} = s_{12} - \frac{s_{12}^2}{s_{11}}, \quad b_{44} = s_{44}, \tag{A10}$$

and s_{11}, s_{12} and s_{44} are material compliance constants. In the text and follows, we use K_{app} to denote the applied mode I stress intensity factor. The relationship between the J-integral, J_{analy}, and the applied mode I stress intensity factor is given by [31]

$$J_{analy} = \frac{K_{app}^2}{\sqrt{2}} b_{11} \left[1 + \frac{2b_{12} + b_{44}}{2b_{11}} \right]^{\frac{1}{2}}. \tag{A11}$$

Without any applied mechanical and/or electrical loads, there are no stresses and electric field in the simulated system due to the homogeneous polarizations. Once polarizations are inhomogeneously distributed, a depolarization field, E_i^d, and an internal stress field, σ_{ij}^{in}, will be generated. Thus, the total electric field is the sum of the applied field plus the depolarization field. The total stress field, σ_{ij}, includes the applied K-field σ_{ij}^a and the internal stress field, σ_{ij}^{in}, i.e.,

$$\sigma_{ij} = \sigma_{ij}^a + \sigma_{ij}^{in}. \tag{A12}$$

The internal stress field is caused by the spontaneous strains. The spontaneous strains at stress-free state, which are called eigenstrains, are associated with the spontaneous polarizations in the following form [26],

$$\begin{aligned}
\varepsilon_{11}^0 &= Q_{11}P_1^2 + Q_{12}(P_2^2 + P_3^2), \\
\varepsilon_{22}^0 &= Q_{11}P_2^2 + Q_{12}(P_3^2 + P_1^2), \\
\varepsilon_{33}^0 &= Q_{11}P_3^2 + Q_{12}(P_1^2 + P_2^2), \\
\varepsilon_{23}^0 &= Q_{44}P_2P_3, \\
\varepsilon_{13}^0 &= Q_{44}P_1P_3, \\
\varepsilon_{12}^0 &= Q_{44}P_1P_2,
\end{aligned} \tag{A13}$$

where Q_{11}, Q_{12} and Q_{44} are the electrostrictive coefficients. Following the thermal stress approach, elastic strains are generated when polarization switching occurs in a perfect mono-domain ferroelectric material, which are calculated by

$$e_{ij} = \varepsilon_{ij} - \Delta\varepsilon_{ij}^{0}, \tag{A14}$$

where $\Delta\varepsilon_{ij}^{0} = Q_{ijkl}(P_k P_l - P_k^0 P_l^0)$ is the change of spontaneous strain after switching, P_i^0 is the initial polarization and ε_{ij} are strains excluding the applied elastic strain, which must be compatible and are defined by

$$\varepsilon_{ij} = \frac{1}{2}(u_{i,j} + u_{j,i}), \tag{A15}$$

in which u_i are displacements. In linear elasticity, stresses are related to elastic strains through Hooke's law:

$$\sigma_{ij}^{in} = c_{ijkl} e_{kl} = c_{ijkl}(\varepsilon_{ij} - \Delta\varepsilon_{ij}^{0}). \tag{A16}$$

Without any body forces, the mechanical equilibrium equations are expressed by $\sigma_{ij,j} = 0$. Since the applied stress field meets the mechanical equilibrium condition, the internal stress field σ_{ij}^{in} should also satisfy the following static mechanical equilibrium equation

$$\sigma_{ij,j}^{in} = 0, \tag{A17}$$

which is solved by the finite element method.

For convenience, we employ the following set of the dimensionless variables for Eq. (3).

$$\mathbf{r}^* = \sqrt{|\alpha_0| / G_{110}}\,\mathbf{r},\ t^* = |\alpha_0| Lt,\ \mathbf{P}^* = \mathbf{P}/P_0,\ \varepsilon_0^* = \varepsilon_0 |\alpha_0|$$

$$\alpha_1^* = \alpha_1 / |\alpha_0|,\ \alpha_{11}^* = \alpha_{11} P_0^2 / |\alpha_0|,\ \alpha_{12}^* = \alpha_{12} P_0^2 / |\alpha_0|,$$

$$\alpha_{111}^* = \alpha_{111} P_0^4 / |\alpha_0|,\ \alpha_{112}^* = \alpha_{112} P_0^4 / |\alpha_0|,\ \alpha_{123}^* = \alpha_{123} P_0^4 / |\alpha_0|,$$

$$Q_{11}^* = Q_{11} P_0^2,\ Q_{12}^* = Q_{12} P_0^2,\ Q_{44}^* = Q_{44} P_0^2,$$

$$s_{11}^{*} = s_{11}(|\alpha_0|P_0^2),\ s_{12}^{*} = s_{12}(|\alpha_0|P_0^2),\ s_{44}^{*} = s_{44}(|\alpha_0|P_0^2),$$

$$G_{11}^{*} = G_{11}/G_{110},\ G_{12}^{*} = G_{12}/G_{110},\ G_{44}^{*} = G_{44}/G_{110},\ G_{44}^{'*} = G_{44}^{'}/G_{110},$$

$$K_{app}^{*} = K_{app}(|\alpha_1|/G_{110})^{1/4}/(|\alpha_1|P_0^2), \tag{A18}$$

where P_0 is the magnitude of the spontaneous polarization at room temperature, G_{110} is a reference value of the gradient energy coefficients, and α_0 represents the value of α_1 at 25ºC. The superscript asterisk, *, denotes the dimensionless value of the corresponding variable. We set the magnitude of the spontaneous polarization at room temperature to be P_0=|**P**$_0$|=0.757 C/m^2, the reference value of the gradient energy coefficients as $G_{110} = 1.73\times10^{-10}\ m^4N/C^2$, the relative dielectric constant, $\kappa = 66.0$, and the value of α_1 at 25ºC to be $\alpha_0 = \alpha_{1,25^\circ\mathrm{C}} = (T - T_0)/(2\varepsilon_0 C_0) = (25 - 479)\times 3.8\times10^5\ \mathrm{m^2N/C^2}$, where T is in units of ºC. The values of the dimensionless (normalized) material coefficients used in the simulations are taken from Reference [19] and listed in Table I.

Table I. Values of the normalized coefficients used in the simulations [19]

α_{11}^{*}	α_{12}^{*}	α_{111}^{*}	α_{112}^{*}	α_{123}^{*}	Q_{11}^{*}	Q_{12}^{*}	Q_{44}^{*}	s_{11}^{*}	s_{12}^{*}	s_{44}^{*}	G_{11}^{*}	G_{12}^{*}	G_{44}^{*}	$G_{44}^{'*}$
-0.24	2.5	0.49	1.2	-7.0	0.05	–0.015	0.038	7.9x10^{-4}	-2.5x10^{-4}	2.08x10^{-3}	0.6	0.0	0.3	0.3

The values of the dimensionless gradient energy coefficients used in the present study are smaller than those used in the pervious work [24]. It was found in the simulations with the higher values of the dimensionless gradient energy coefficients that polarization switching was very difficult to occur near the crack tip and the numerical iteration was often divergent. A systematic investigation is needed to clarify the role of the values of the dimensionless gradient energy coefficients in the polarization switching-induced toughening.

With the dimensionless variables we explicitly express the 2D time-dependent Ginzburg-Landau equation, i.e., Eq. (3), as:

$$\begin{aligned}\frac{\partial P_1^*}{\partial t^*} = -[&2\alpha_1^* P_1^* + 4\alpha_{11}^* P_1^{*3} + 2\alpha_{12}^* P_1^* P_2^{*2} + 6\alpha_{111}^* P_1^{*5} + \alpha_{112}^*(4P_1^{*3}P_2^{*2} + 2P_1^* P_2^{*4}) \\ &- 2Q_{11}^*\sigma_{11}P_1^* - 2Q_{12}^*\sigma_{22}P_1^* - Q_{44}^*\sigma_{12}P_2^* \\ &- G_{11}^* P_{1,11}^* - (G_{12}^* + G_{44}^* - G_{44}^{'*})P_{2,12}^* - (G_{44}^* + G_{44}^{'*})P_{1,22}^* - \tfrac{1}{2}E_1^{d*} - E_1^{a*}],\end{aligned} \tag{A19a}$$

$$\begin{aligned}\frac{\partial P_2^*}{\partial t^*} = -[&2\alpha_1^* P_2^* + 4\alpha_{11}^* P_2^{*3} + 2\alpha_{12}^* P_2^* P_1^{*2} + 6\alpha_{111}^* P_2^{*5} + \alpha_{112}^*(4P_2^{*3}P_1^{*2} + 2P_2^* P_1^{*4}) \\ &- 2Q_{11}^*\sigma_{22}P_2^* - 2Q_{12}^*\sigma_{11}P_2^* - Q_{44}^*\sigma_{12}P_1^* \\ &- G_{11}^* P_{2,22}^* - (G_{12}^* + G_{44}^* - G_{44}^{'*})P_{1,12}^* - (G_{44}^* + G_{44}^{'*})P_{2,11}^* - \tfrac{1}{2}E_2^{d*} - E_2^{a*}].\end{aligned} \tag{A19b}$$

The finite difference method for spatial derivatives and the Runge-Kutta method of order four for temporal derivatives are employed to solve Eq. (A19) in real space with the free boundary condition.

References

[1] Park SB, Sun CT. J Am Ceram Soc 1995;78:1475.

[2] Wang H, Singh RN. J Appl Phys 1997;81:7471.

[3] Fu R, Zhang TY. J Am Ceram Soc 2000;83:1215.

[4] Fu R, Zhang TY. Acta Mater 2000;48:1729.

[5] Zhang TY, Zhao MH, Tong P. Adv Appl Mech 2002; 38:147.

[6] McMeeking RM, Evans AG. J Am Ceram Soc 1982;65:242.

[7] Fulton CC, Gao, H. Acta Mater 2001;49:2039.

[8] Hwang SC, Lynch CS, McMeeking RM. Acta Metall Mater 1995;43:2073.

[9] Landis CM. J Mech Phys Solids 2003;51:1347.

[10] Beom HG, Atluri SN. J Mech Phys Solids 2003;51:1107.

[11] Zhu T, Yang W. Acta Mater 1997;45:4695.

[12] Rajapakse RKND, Zeng X. Acta Mater 2001;49: 877.

[13] Huber JE, Fleck NA, Landis CM, McMeeking RM. J Mech Phys Solids 1999;47: 1663.

[14] Zhang TY, Gao CF. Theo Appl Frac Mech 2004;41:339.

[15] Schneider GA, Felten F, McMeeking RM. Acta mater 2003;51:2235.

[16] Zhang W, Bhattacharya K. Acta Mater 2005;53:199.

[17] Wang J, Shi SQ, Chen LQ, Li YL, Zhang TY. Acta Mater 2004;52:749.

[18] Wang J, Li YL, Chen LQ, Zhang TY. Acta Mater 2005;53:2495.

[19] Li YL, Hu SY, Liu ZK, Chen LQ. Acta Mater 2002;50:395.

[20] Nambu S, Sagala DA. Phys Rev B 1994;50:5838.

[21] Hu HL, Chen LQ. J Am Ceram Soc 1998;81:492.

[22] Cao W, Tavener S, Xie S. J Appl Phys 1999;86:5739.

[23] Zhang W, Bhattacharya K. Acta Mater 2005;53:185.

[24] Wang J, Zhang TY. Phys Rev B 2006;73:144107

[25] Dugdale DS. J Mech Phys Solids 1960;8:100

[26] Lines ME, Glass AM. Principles and applications of ferroelectrics and related materials, (Clarendon press, Oxford, 1977).

[27] Haun MJ, Furman E, Jang SJ, McKinstry HA, Closs LE. J. Appl. Phys. 1987;62:3331.

[28] Wang YG, Zhong WL, Zhang PL. Phys Rev B 1995;51:5311.

[29] Kretschmer R, and Binder K, Phys Rev B 1979;20:1065.

[30] Li YL, Hu SY, Liu ZK, Chen LQ. Appl Phys Lett 2002;81:427.

[31] Sih GC, Liebowitz H. in "Fracture: An advanced Treatise", ed. by Liebowitz H., Vol. II (Academic Press, New York and London, 1968)

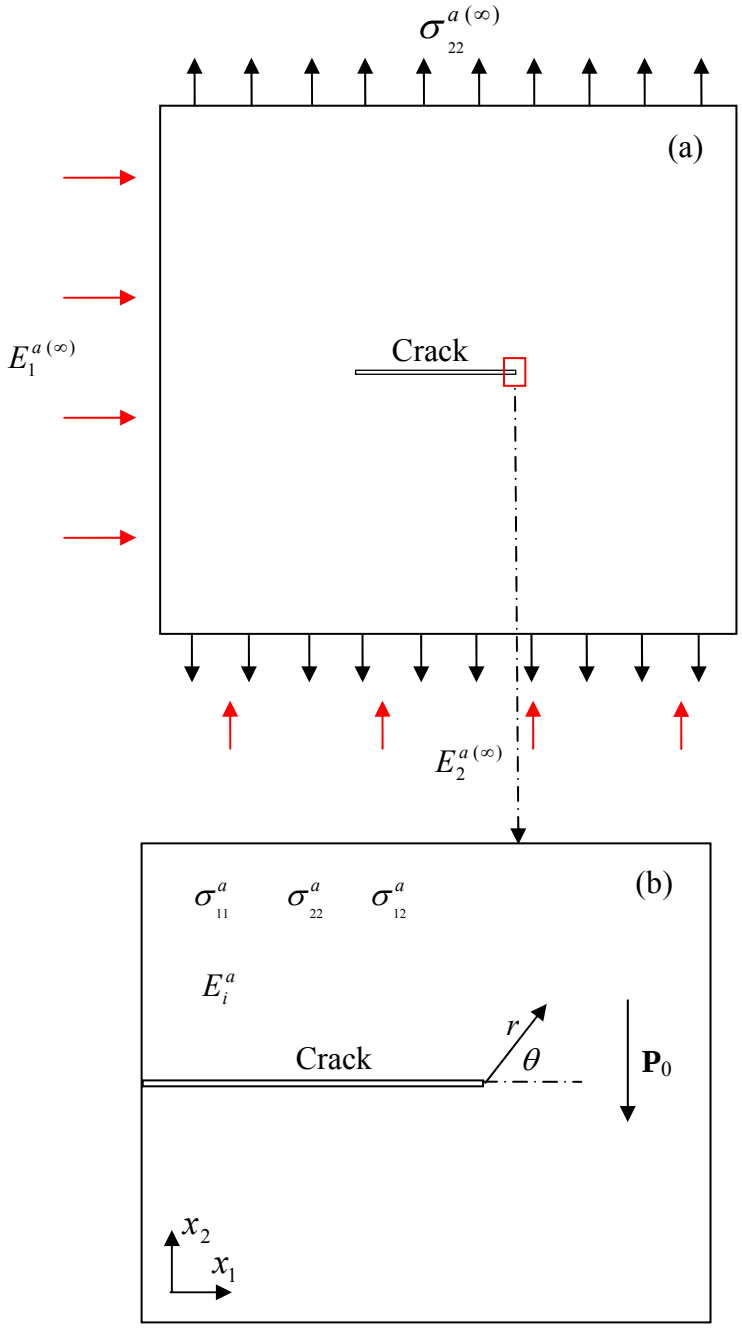

Fig.1 Schematic illustration of an electrically permeable crack in a mono-domain ferroelectric: (a) crack in infinite medium under combined remote loadings; (b) simulated crack tip area subjected to applied K-field stresses of mode I and a uniform electric field of E_i^a, where P_0 indicating the poling direction.

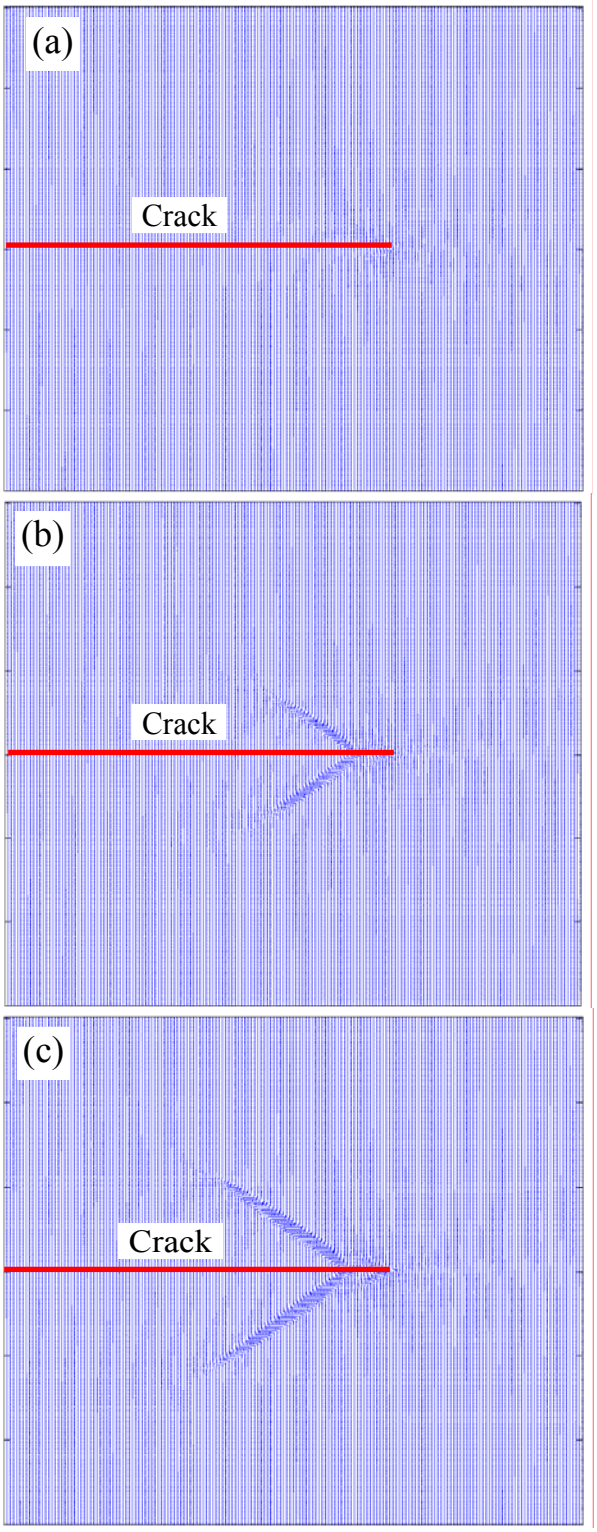

Fig.2 Polarization distribution under (a) $K_{app}^{*}=440$, (b) $K_{app}^{*}=500$ and (c) $K_{app}^{*}=560$, without any applied electric field.

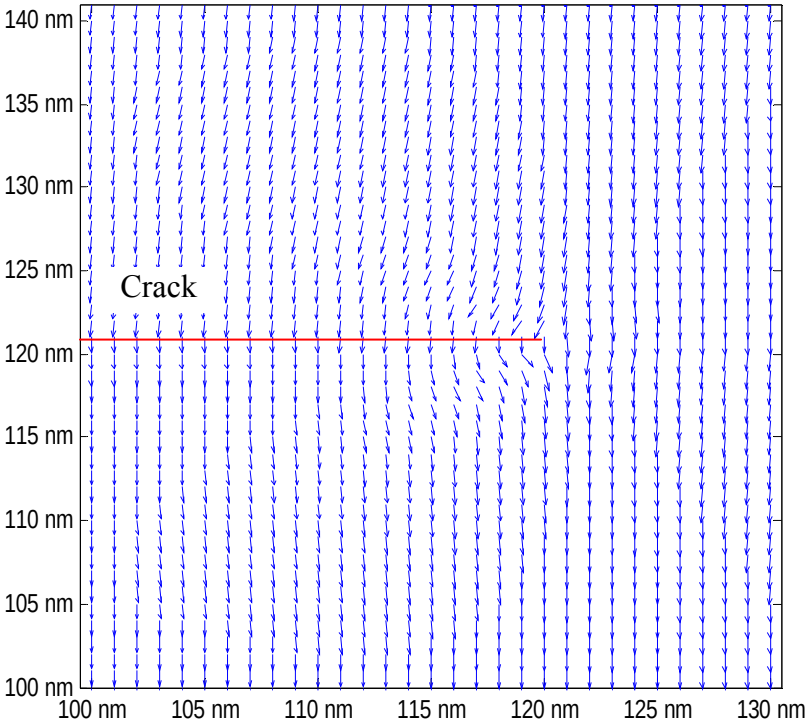

Fig.3 The detailed polarization distribution near the crack tip in Fig. 2 (a).

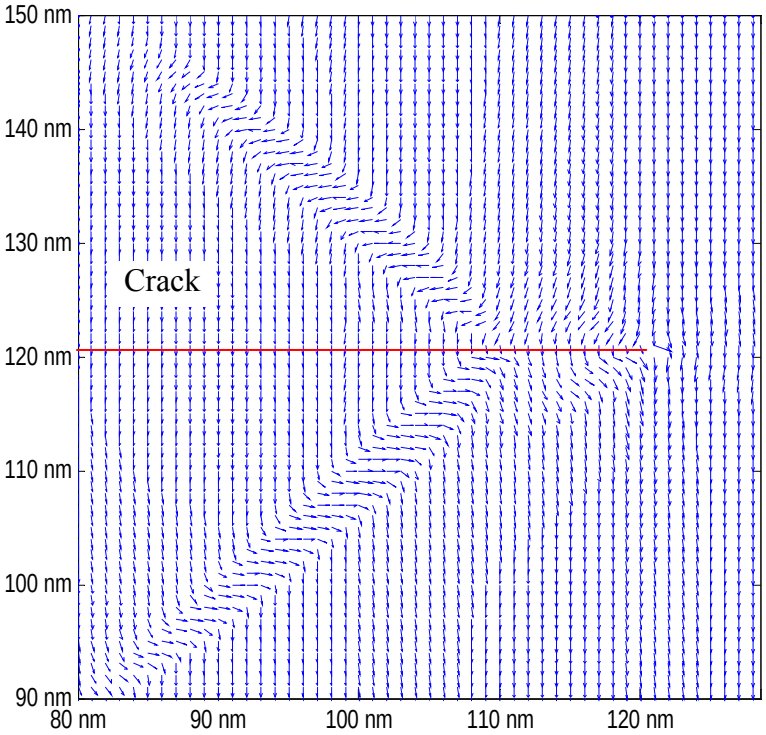

Fig.4 The detailed polarization distribution near the crack tip in Fig. 2 (b).

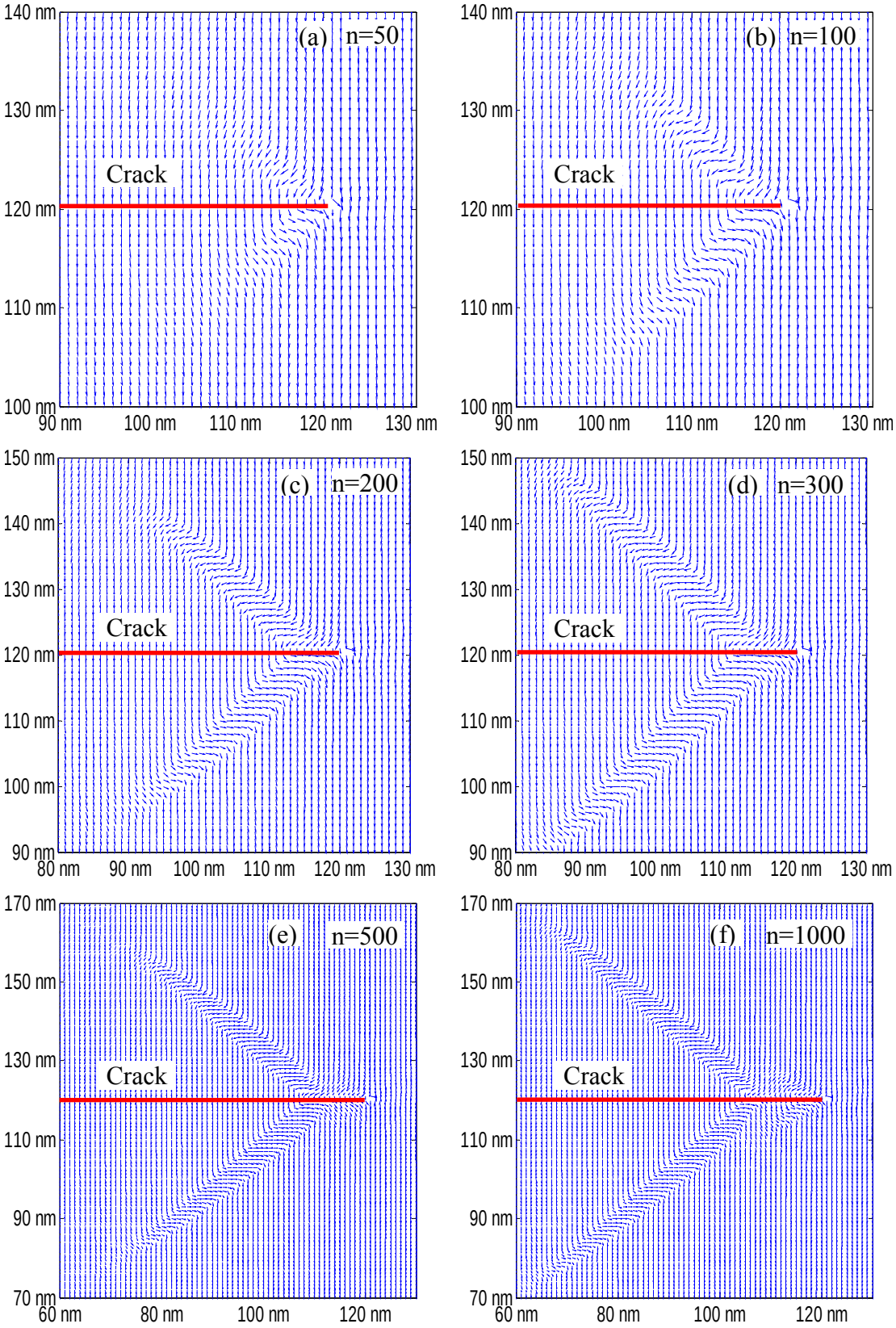

Fig.5 Temporal evolution of polarization switching at different time steps n under $K^{*}_{app} = 560$ without any applied electric field.

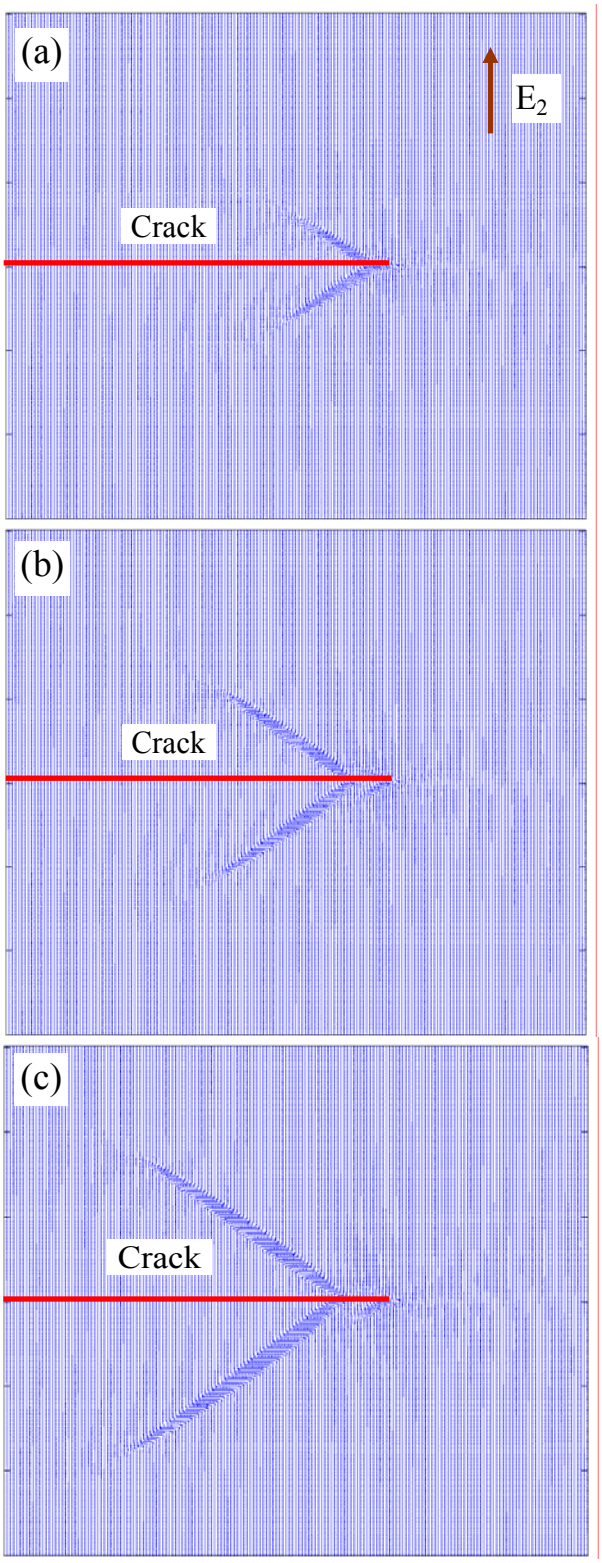

Fig.6 Polarization distribution under (a) $K^*_{app} = 560$ and $E_2^{a,*} = -0.5$, (b) $K^*_{app} = 560$ and $E_2^{a,*} = 0$, and (c) $K^*_{app} = 560$ and $E_2^{a,*} = 0.5$.

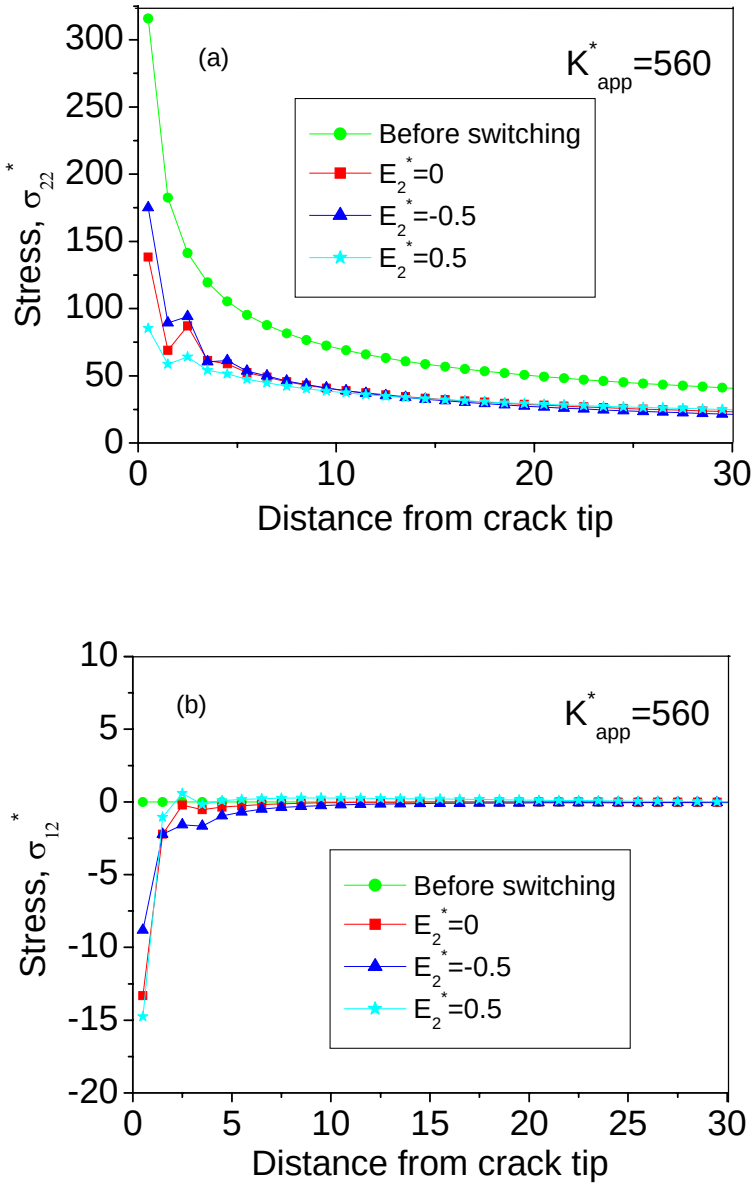

Fig. 7 Stresses distribution in front of the crack tip with θ=0 before and after switching. The curve with solid circles denotes the applied stress. The curves with solid triangles, solid rectangles and solid stars represent the total stresses after switching under $K^*_{app} = 560$ and uniform electric fields of $E_2^{a,*} = -0.5$, $E_2^{a,*} = 0$, and $E_2^{a,*} = 0.5$, respectively.

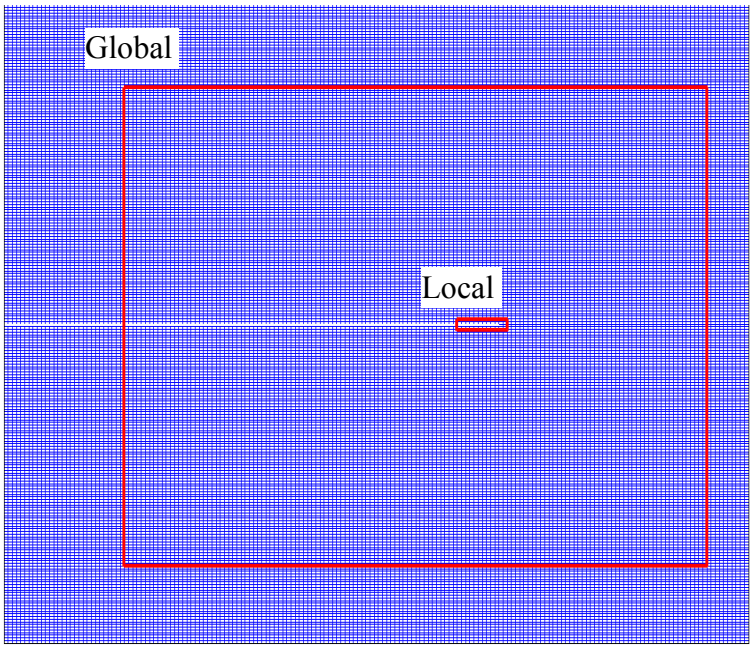

(a) Global contour and local contour

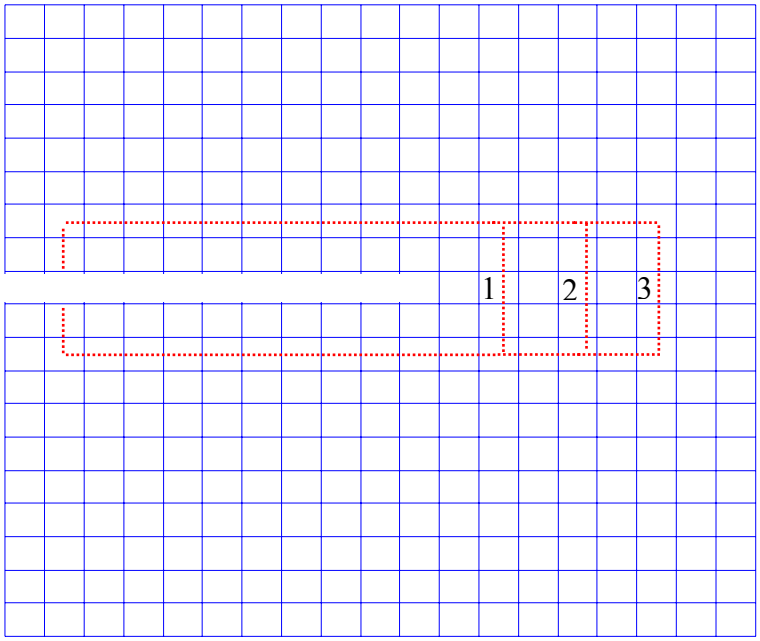

(b) Different local contours

Fig. 8 The illustration of different J-integral contours around the crack tip. Contour 2 in (b) is the same as the local contour in (a)

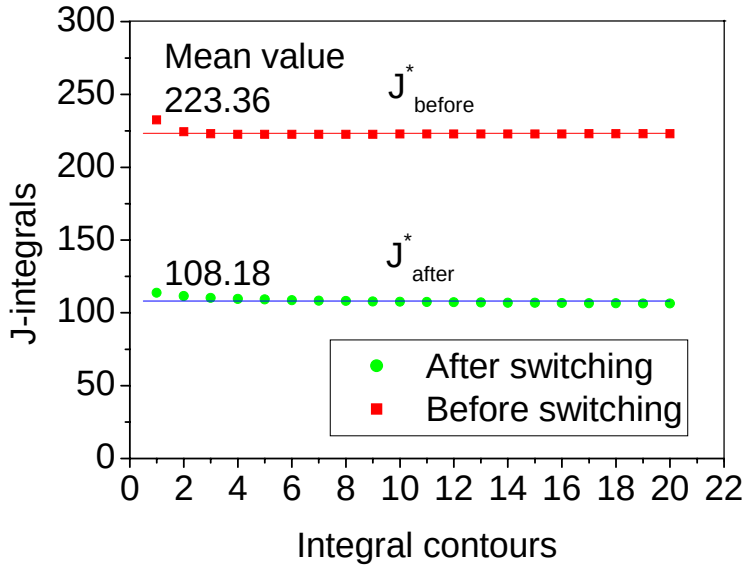

Fig. 9 The mechanical part of J-integrals obtained from different integral contours before and after polarization switching under purely mechanical load of $K^*_{app} = 560$.

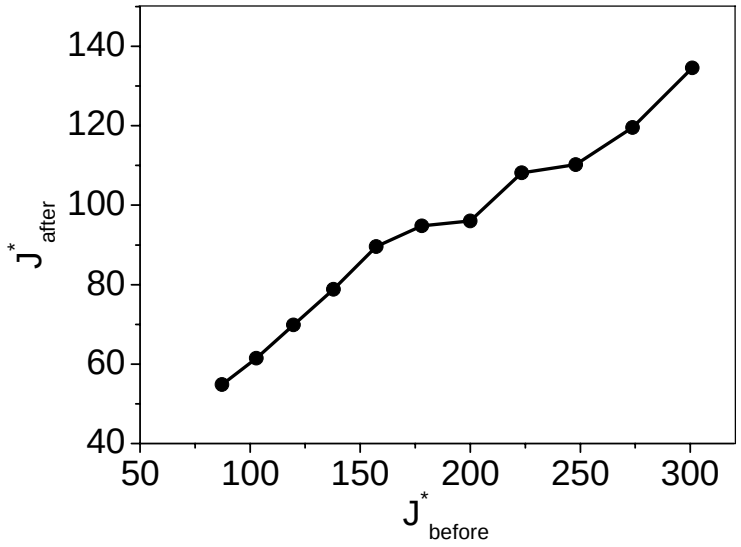

Fig. 10 Local J-integral after switching versus local J-integral before switching without electric field.

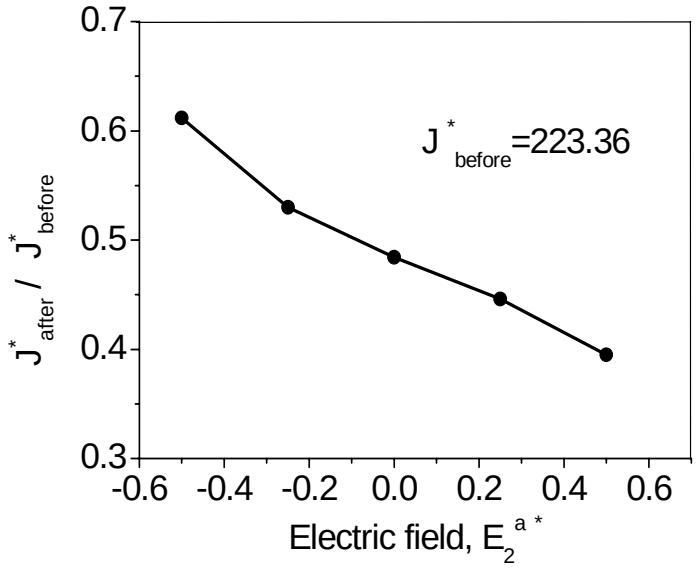

Fig.11 Local J-integral variation under different uniform electric fields.

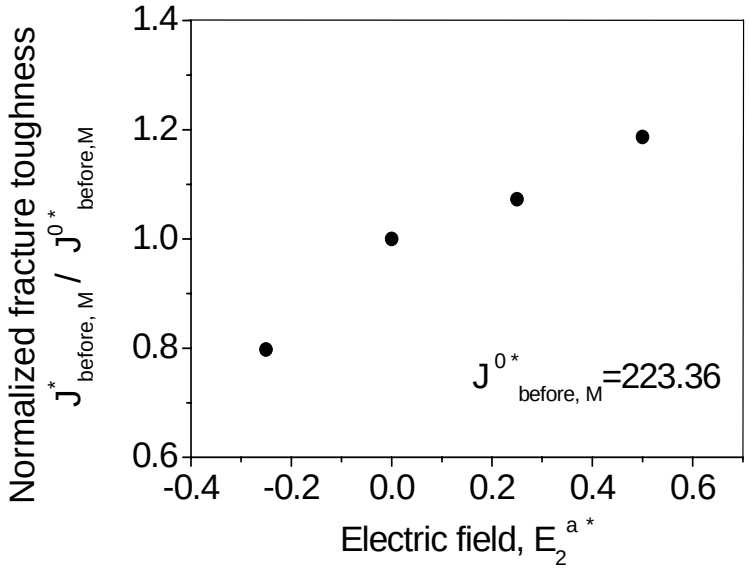

Fig. 12 Effects of uniform electric fields on the fracture toughness of the model ferroelectric.

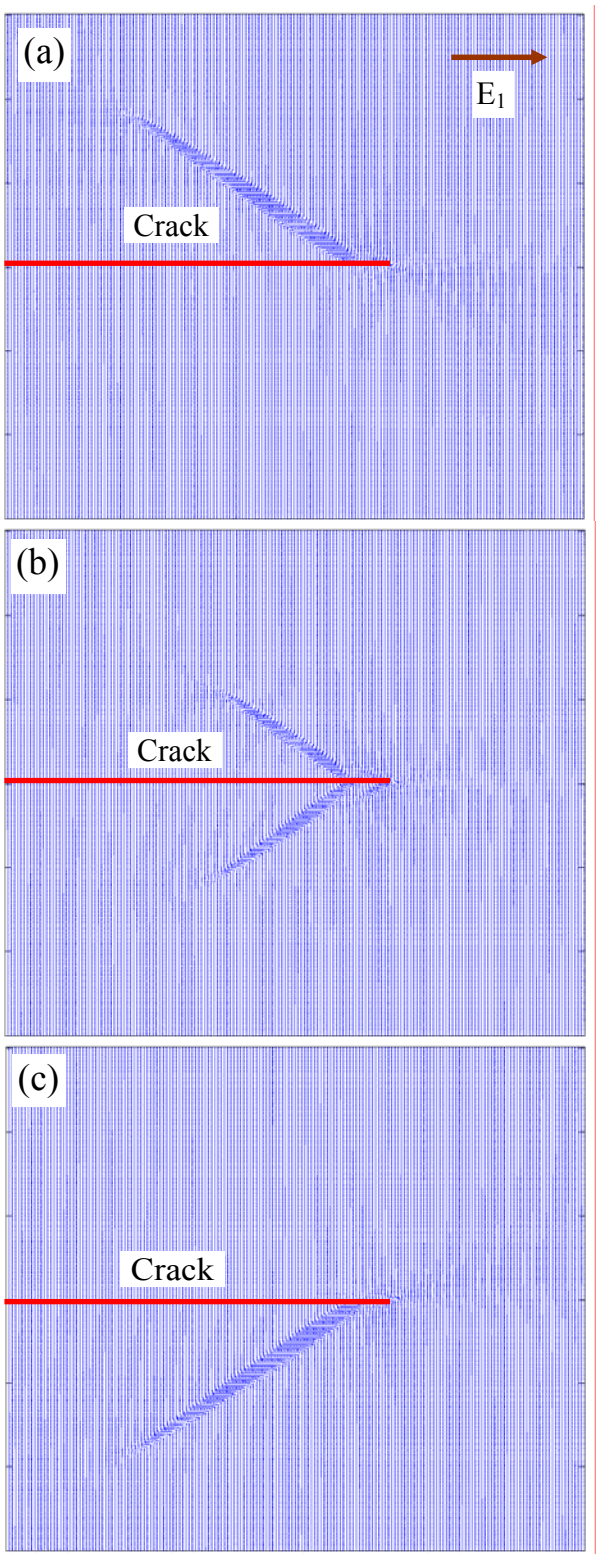

Fig.13 Polarization distribution under $K^*_{app} = 560$ and applied electric field (a) $E_1^{a*} = -0.25$, (b) $E_1^{a*} = 0$, and (c) $E_1^{a*} = 0.25$.

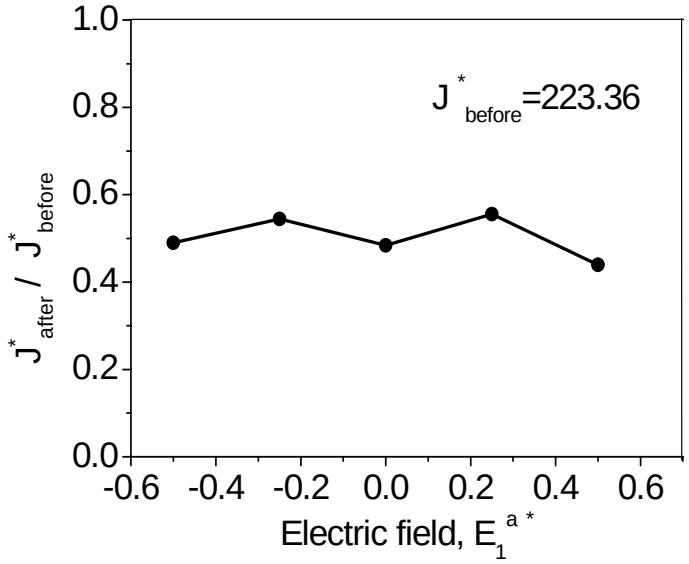

Fig.14 Local J-integral variation under different uniform electric fields perpendicular to poling direction.